# Electronic Supplementary Information (ESI)

## Synthesis, structure and characterization of new dithiocarbazate based mixed ligand oxidovanadium(IV) complexes: DNA/HSA interaction, cytotoxic activity and DFT studies

Atanu Banerjee,[a] Monalisa Mohanty,[a] Sudhir Lima,[a] Rajib Samanta,[a] Eugenio Garribba,[b] Takahiro Sasamori,[c] and Rupam Dinda*[,a]

[a] *Department of Chemistry, National Institute of Technology, Rourkela, 769008 Odisha, India*

[b] *Dipartimento di Chimica e Farmacia, Università di Sassari, Via Vienna 2, I-07100 Sassari, Italy*

[c] *Graduate School of Natural Sciences, Nagoya City University Yamanohata 1, Mizuho-cho, Mizuho-ku, Nagoya, Aichi 467-8501, Japan*

**Table S1**. Selected bond lengths (Å) and bond angles (°) for experimental (exptl.) and calculated (calcd.) structures of $[V^{IV}OL^{1}(phen)]$ (**1**), $[V^{IV}OL^{2}(phen)]$ (**2**) and $[V^{IV}OL^{1}(bipy)]$ (**3**)**,** using the functional B3P86 and the general basis set with 6-311g on V, O, C, H and N atoms and 6311+g(d) on S and Cl.[a,b]

| | $[V^{IV}OL^{1}(phen)]$ (**1**) | | $[V^{IV}OL^{2}(phen)]$ (**2**) | | $[V^{IV}OL^{1}(bipy)]$ (**3**) | |
|---|---|---|---|---|---|---|
| Distance/Angle | Exptl. | Calcd. | Exptl. | Calcd. | Exptl. | Calcd. |
| V(1)–O(1) | 1.591 | 1.604 | 1.603 | 1.604 | 1.597 | 1.605 |
| V(1)–O(2) | 1.949 | 1.946 | 1.954 | 1.937 | 1.951 | 1.947 |
| V(1)–N(2) | 2.047 | 2.058 | 2.061 | 2.062 | 2.057 | 2.059 |
| V(1)–N(4) | 2.145 | 2.140 | 2.135 | 2.142 | 2.137 | 2.145 |
| V(1)–N(3) | 2.316 | 2.347 | 2.342 | 2.352 | 2.314 | 2.305 |
| V(1)–S(1) | 2.431 | 2.422 | 2.409 | 2.431 | 2.419 | 2.422 |
| O(1)–V(1)–O(2) | 101.9 | 102.2 | 100.6 | 103.0 | 100.9 | 102.1 |
| O(1)–V(1)–N(2) | 104.4 | 106.0 | 104.1 | 105.3 | 103.1 | 105.3 |
| O(2)–V(1)–N(2) | 85.9 | 85.4 | 88.9 | 87.4 | 85.5 | 85.3 |
| O(1)–V(1)–N(4) | 91.8 | 90.8 | 94.6 | 90.8 | 93.7 | 90.3 |
| O(2)–V(1)–N(4) | 92.2 | 93.8 | 91.9 | 91.7 | 89.4 | 94.1 |
| N(2)–V(1)–N(4) | 163.8 | 162.9 | 160.9 | 163.7 | 163.1 | 164.2 |
| O(1)–V(1)–N(3) | 164.9 | 163.5 | 167.7 | 163.4 | 165.6 | 162.0 |
| O(2)–V(1)–N(3) | 80.2 | 79.3 | 79.1 | 79.0 | 80.7 | 79.3 |
| N(2)–V(1)–N(3) | 90.6 | 90.4 | 88.3 | 91.2 | 91.2 | 92.7 |
| N(4)–V(1)–N(3) | 73.2 | 72.7 | 73.1 | 72.6 | 72.0 | 71.8 |
| O(1)–V(1)–S(1) | 98.6 | 100.6 | 98.9 | 99.8 | 98.9 | 100.7 |
| O(2)–V(1)–S(1) | 158.0 | 156.2 | 159.7 | 156.5 | 157.9 | 156.0 |
| N(2)–V(1)–S(1) | 81.3 | 81.7 | 80.8 | 81.2 | 80.3 | 81.6 |
| N(4)–V(1)–S(1) | 95.1 | 92.7 | 92.3 | 93.6 | 99.3 | 93.1 |
| N(3)–V(1)–S(1) | 82.1 | 80.8 | 83.1 | 80.8 | 82.7 | 81.3 |
| **MAPD (distance)**[c] | **0.6** | | **0.4** | | **0.3** | |
| **MAPD (angle)**[c] | **1.1** | | **1.7** | | **2.1** | |

[a] The numbers of the atoms are the same as in **Figure 2** of the main text. [b] Distances in Å and angles in degrees. [c] Mean absolute percent deviation.

**Table S2**. Spin Hamiltonian parameters calculated by DFT methods from first principles for oxidovanadium(IV) complexes **1–3**.[a]

| Complex | $g_{iso}$ | $g_x$ | $g_y$ | $g_z$ | $A_{iso}$ | $A_x$ | $A_y$ | $A_z$ |
|---|---|---|---|---|---|---|---|---|
| [$V^{IV}OL^1$(phen)] (**1**) | 1.978 | 1.985 | 1.983 | 1.966 | -85.3 | -51.9 | -52.8 | -151.3 |
| [$V^{IV}OL^2$(phen)] (**2**) | 1.978 | 1.984 | 1.982 | 1.967 | -85.4 | -52.0 | -52.7 | -151.4 |
| [$V^{IV}OL^1$(bipy)] (**3**) | 1.978 | 1.985 | 1.982 | 1.966 | -85.6 | -52.2 | -53.3 | -151.5 |

[a] $A$ values reported $10^{-4}$ $cm^{-1}$ units.

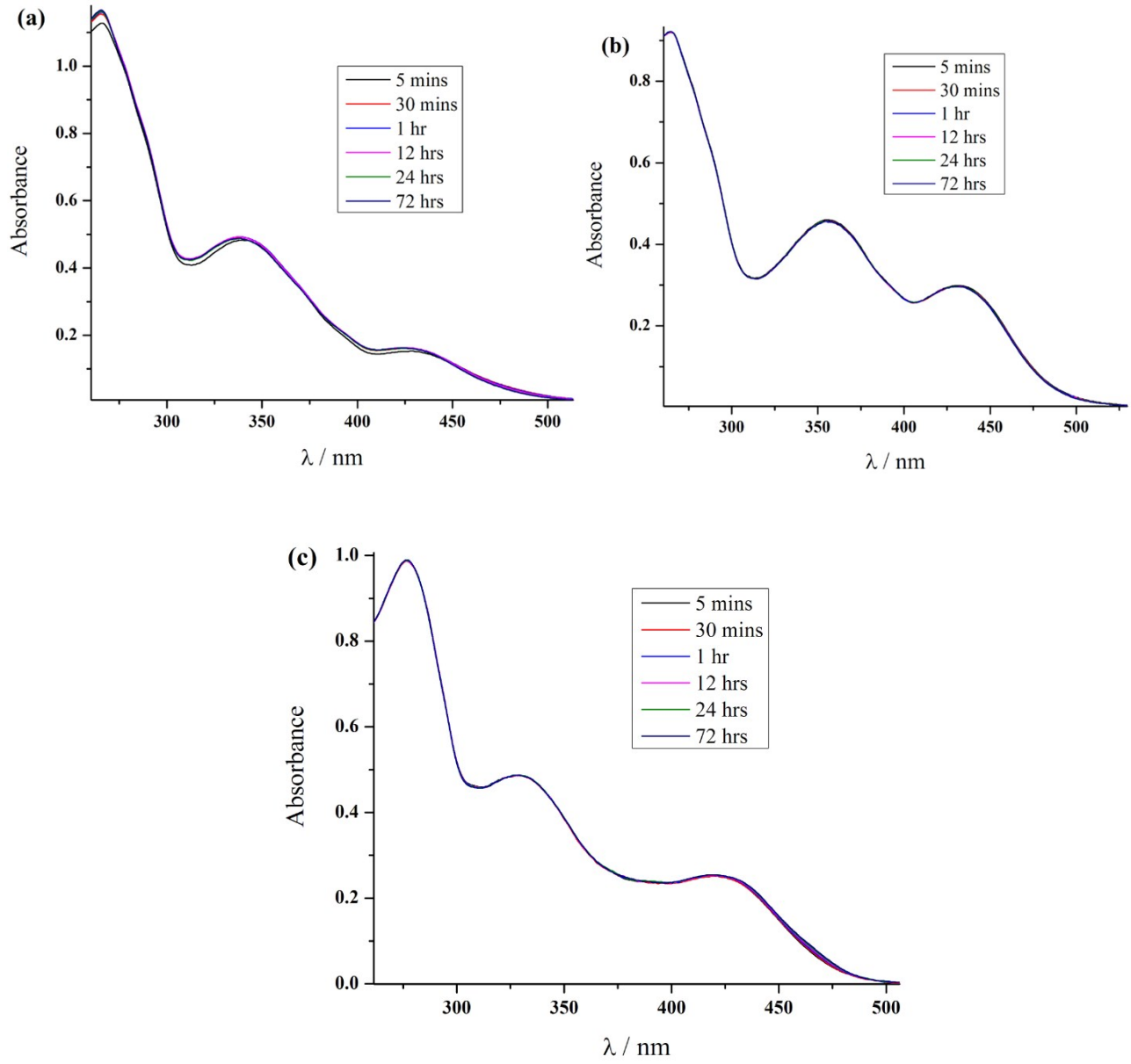


**Figure S1**. Time dependent UV/vis spectra of [$V^{IV}OL^1$(phen)] (**1**) (a), [$V^{IV}OL^2$(phen)] (**2**) (b) and [$V^{IV}OL^1$(bipy)] (**3**) (c) in Tris-HCl buffer.

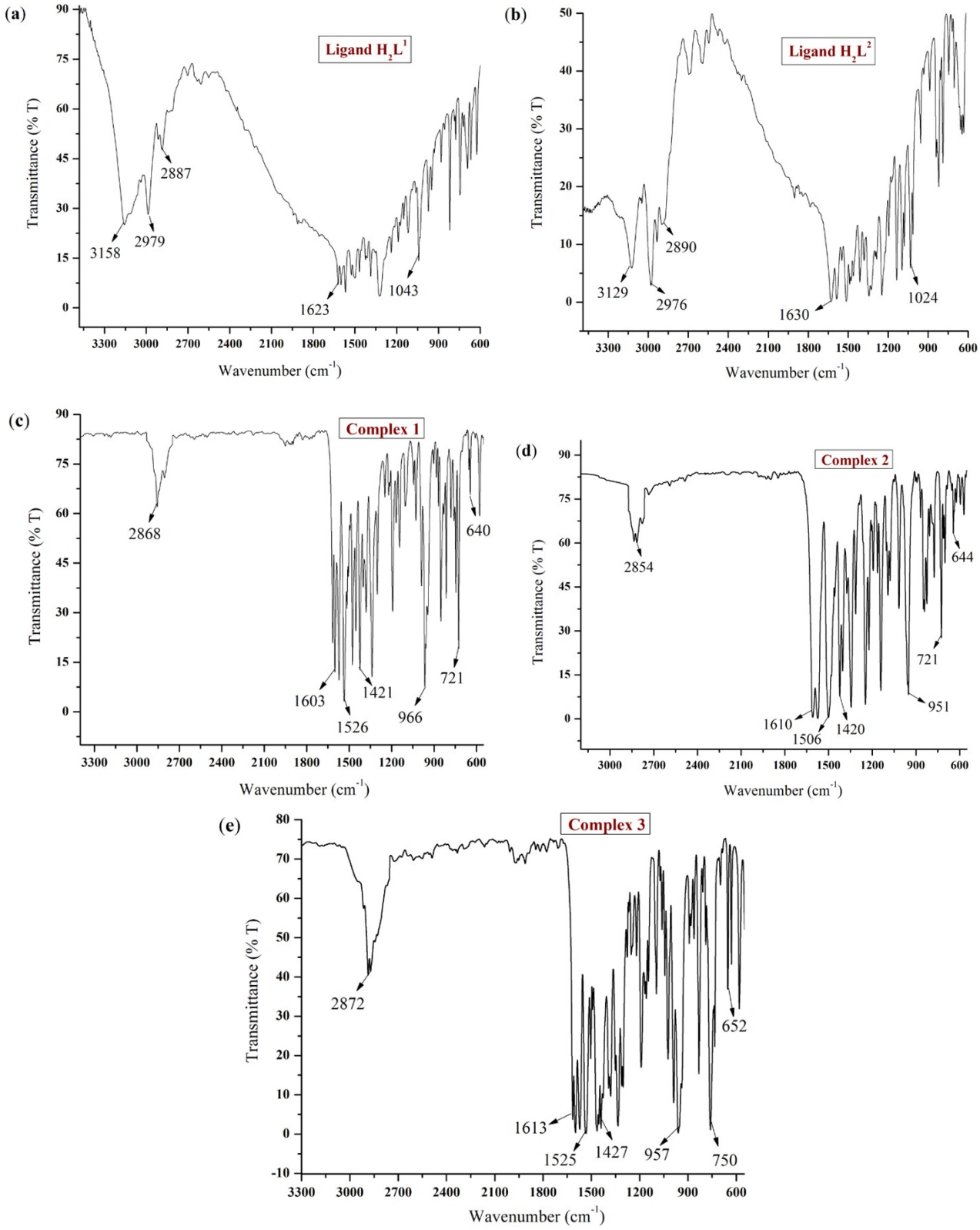


**Figure S2**. IR spectrum of ligand $H_2L^1$ (a) and $H_2L^2$ (b) and and their corresponding complexes $[V^{IV}OL^1(phen)]$ (**1**) (c), $[V^{IV}OL^2(phen)]$ (**2**) (d) and $[V^{IV}OL^1(bipy)]$ (**3**) (e) in KBr.

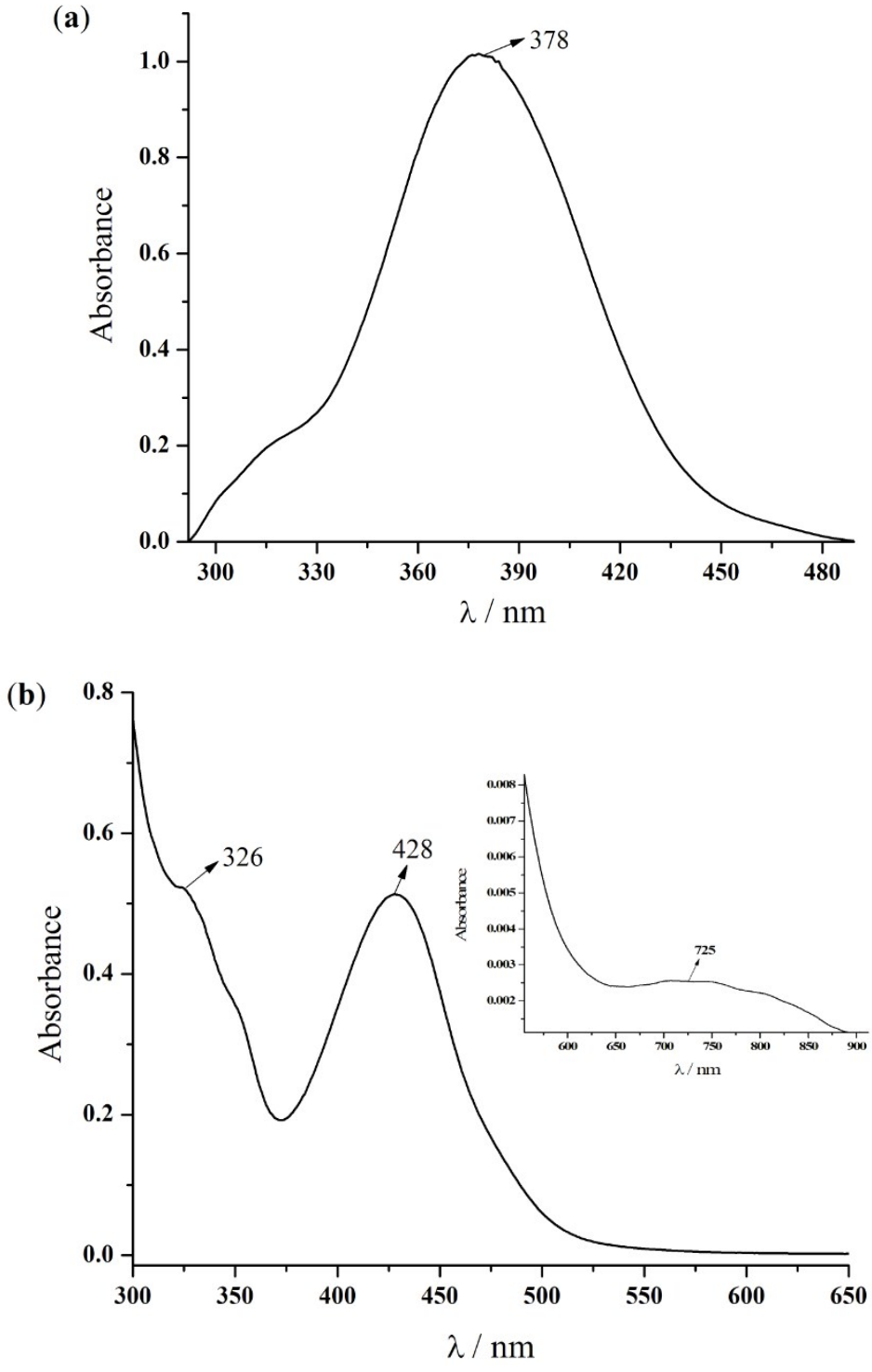


**Figure S3**. UV/vis spectra of ligand $H_2L^1$ (a) and complex [$V^{IV}OL^1$(phen)] (**1**) (b) ($1.8 \times 10^{-4}$ M) recorded in DMSO.

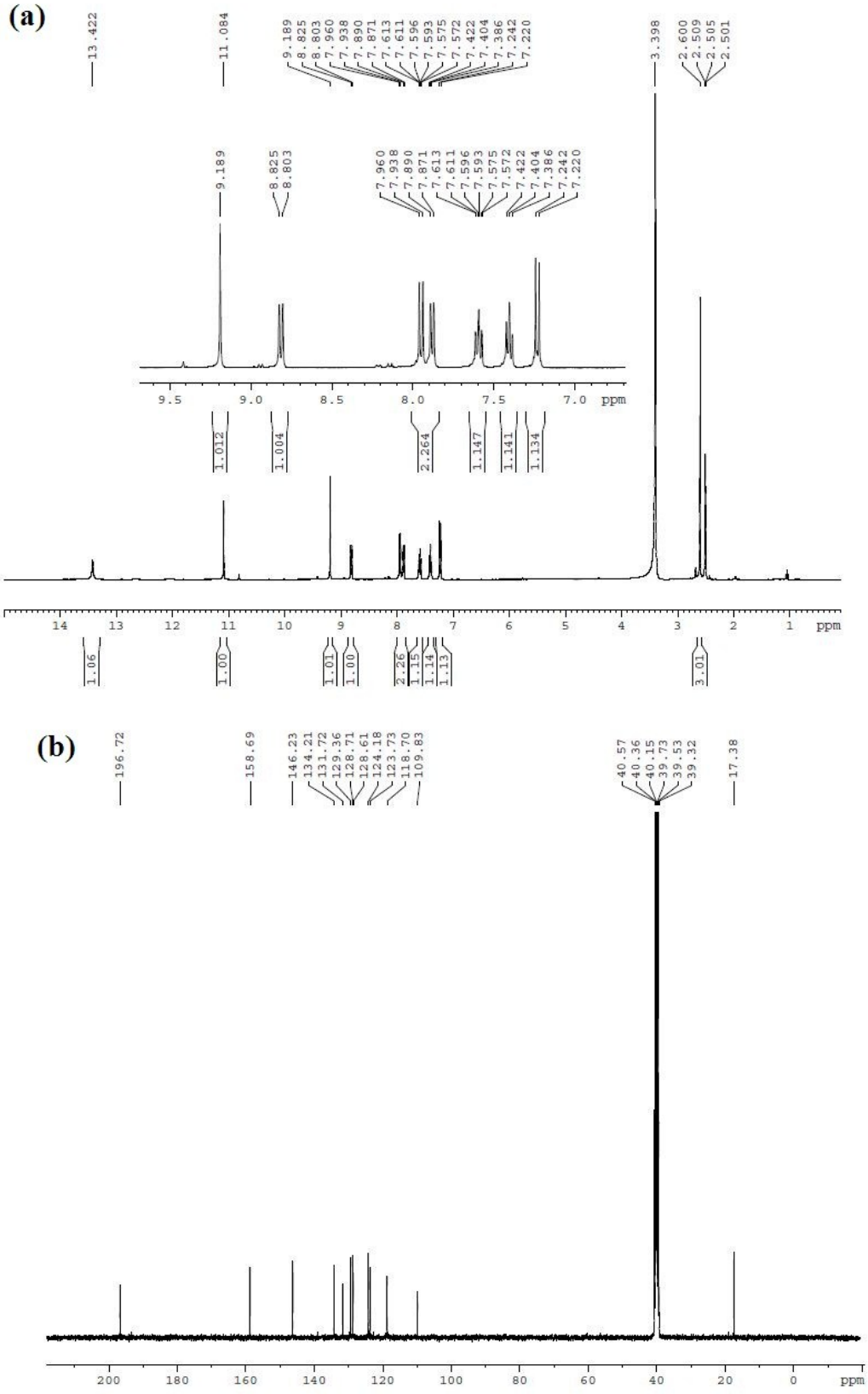


**Figure S4**. $^{1}H$ NMR (a) and $^{13}C$ NMR (b) spectrum of ligand $H_2L^1$ in DMSO-$d_6$

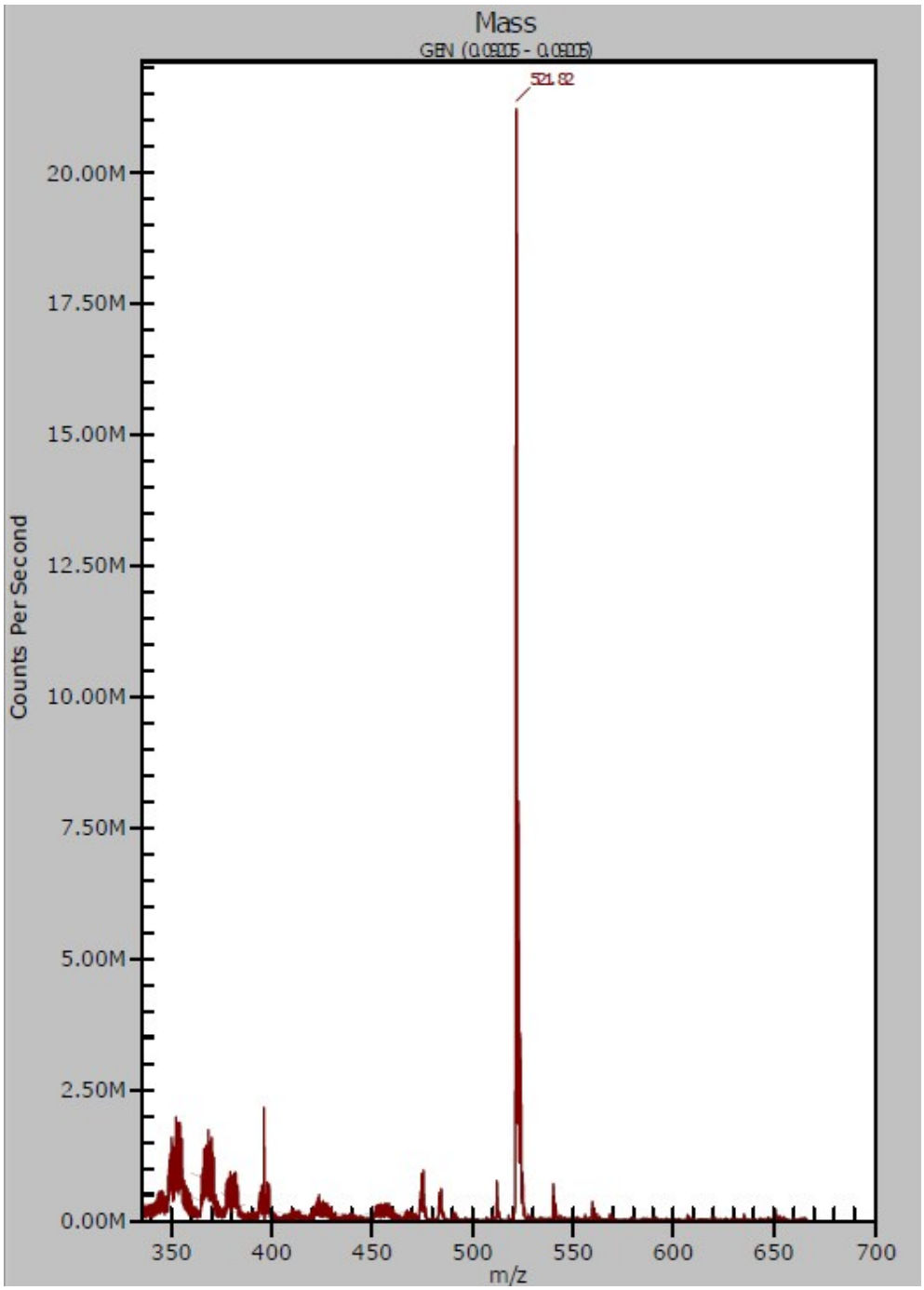


**Figure S5**. ESI–MS spectrum of [$V^{IV}OL^{1}$(phen)] (**1**) recorded in in $CH_3CN$ (100 pmol/µL) at positive ion mode.

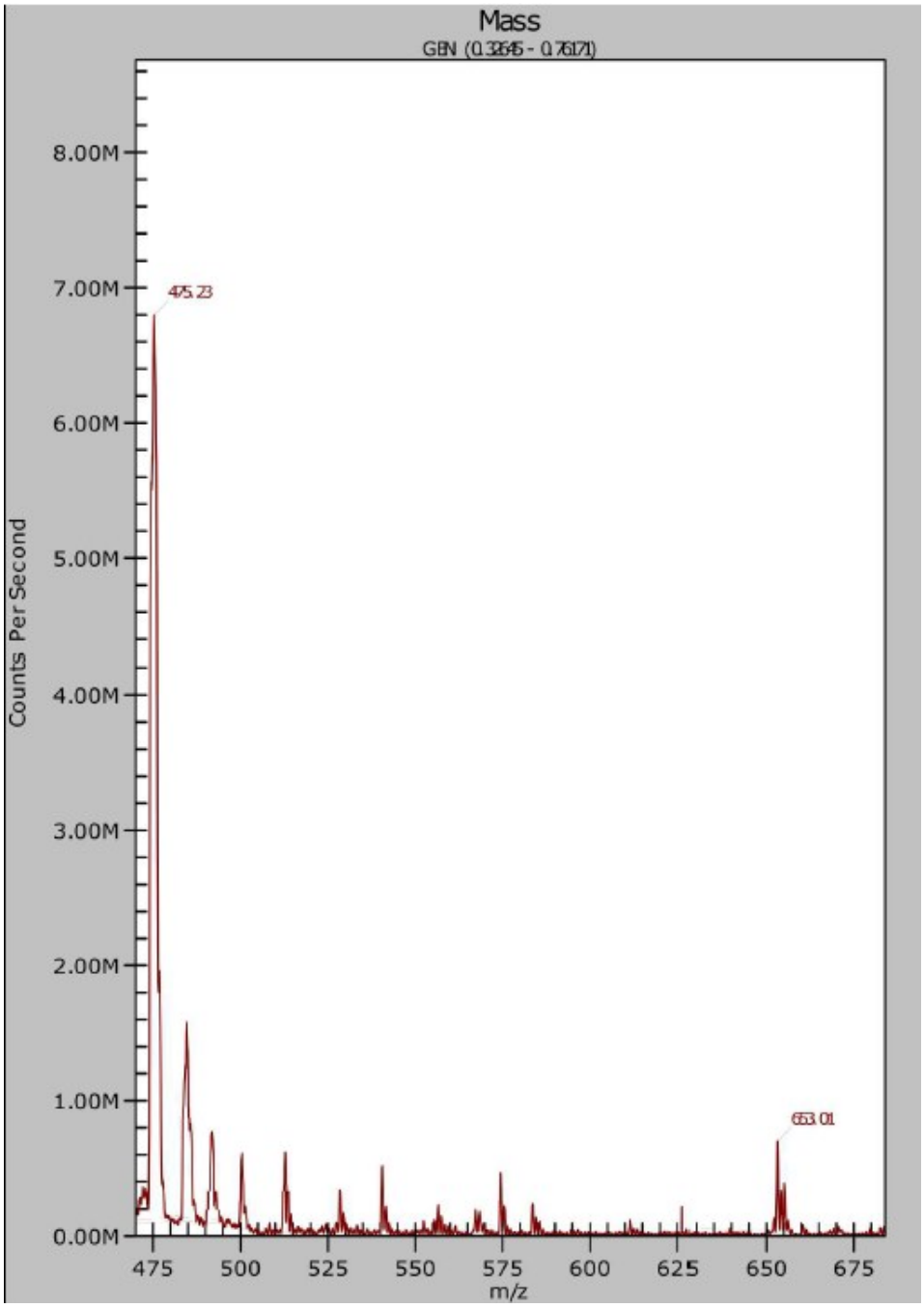


**Figure S6**. ESI–MS spectrum of [$V^{IV}OL^2$(phen)] (**2**) recorded in in $CH_3CN$ (100 pmol/µL) at positive ion mode.

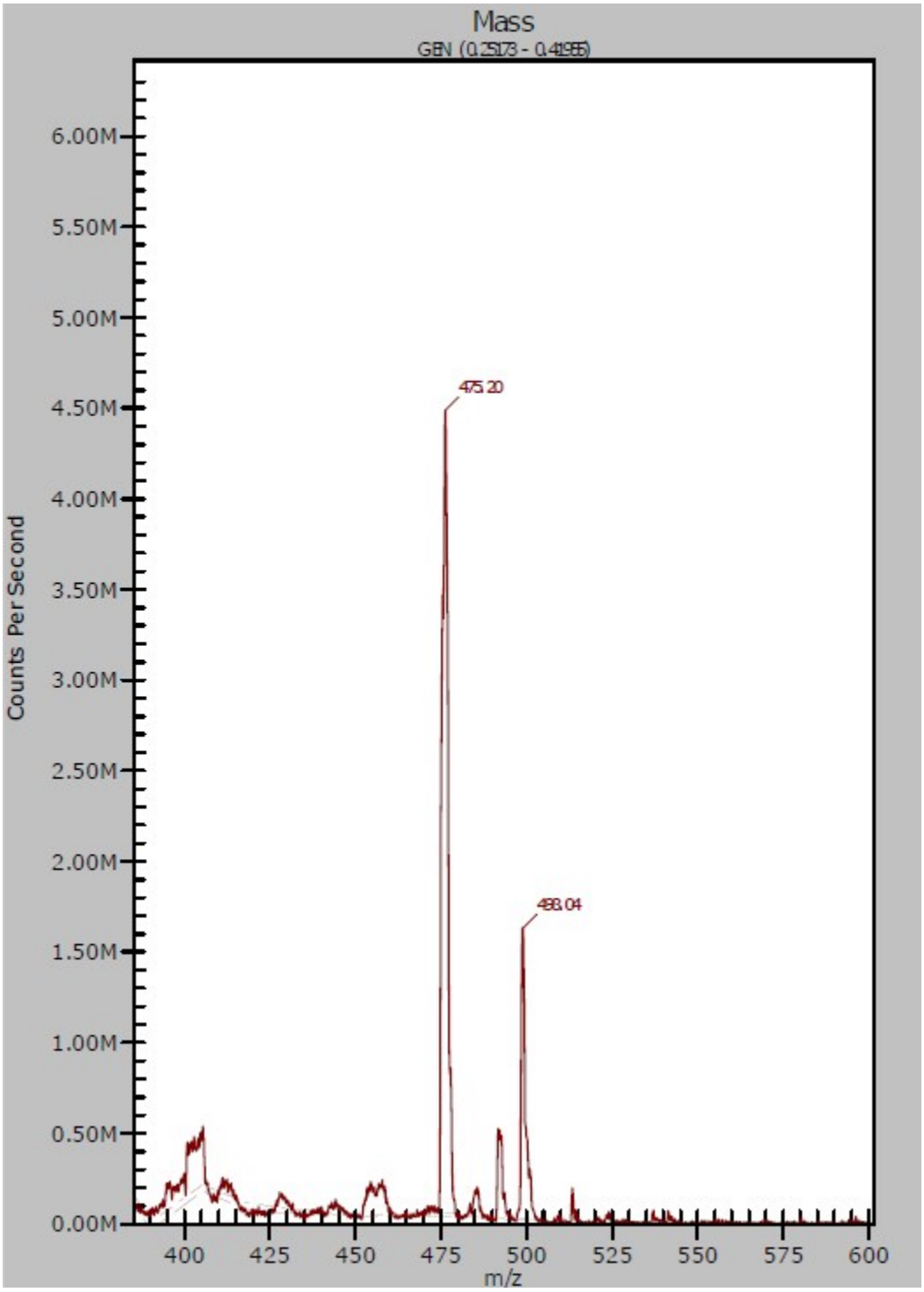


**Figure S7**. ESI–MS spectrum of [$V^{IV}OL^{1}$(bipy)] (**3**) recorded in in $CH_3CN$ (100 pmol/µL) at positive ion mode.

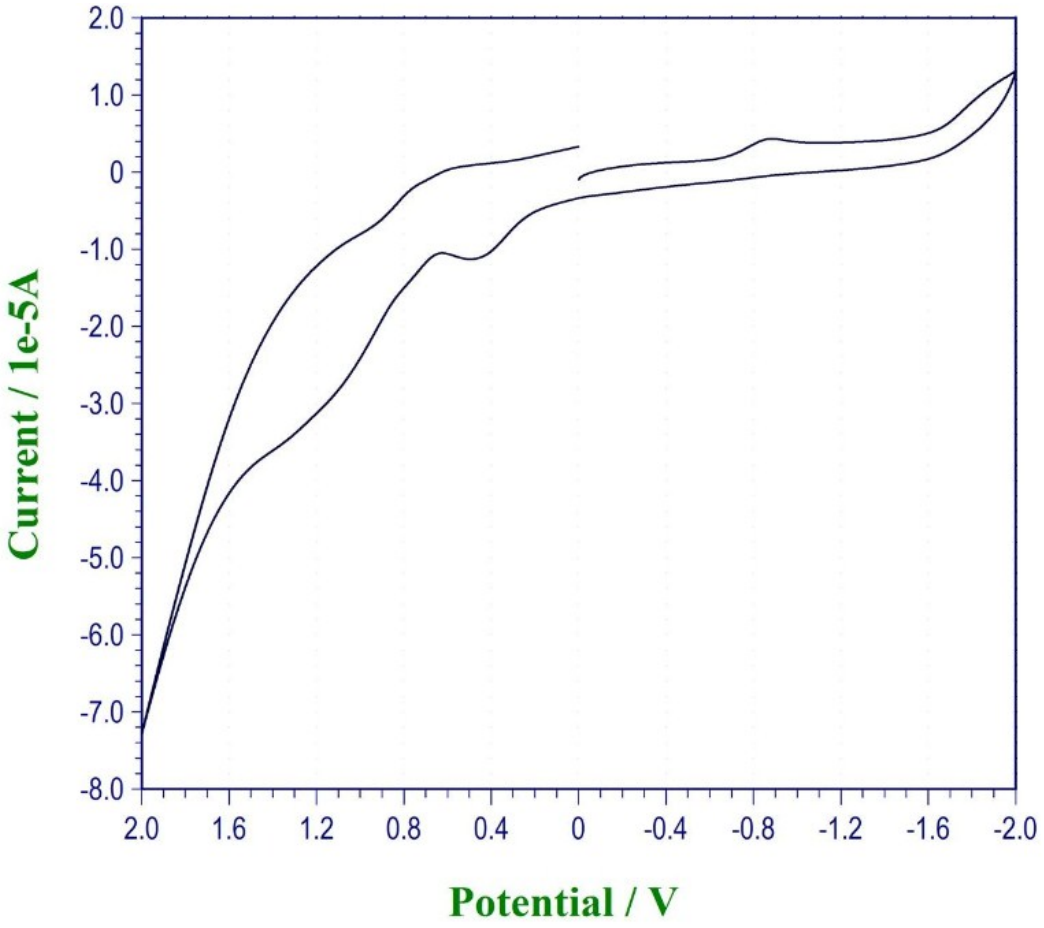


**Figure S8.** Cyclic voltammogram of $H_2L^1$ ($10^{-4}$ M) obtained in DMSO at a scan rate of 200 mV $s^{-1}$.

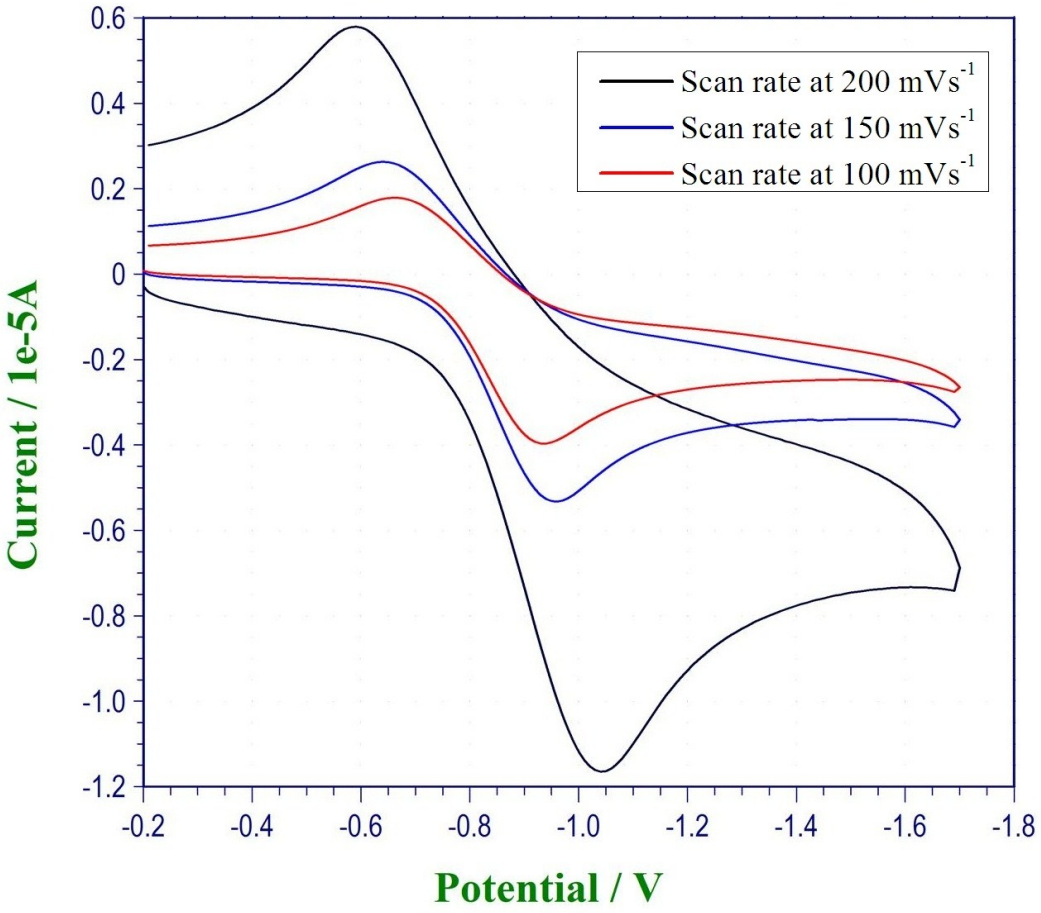


**Figure S9**. Cyclic voltammogram of [$V^{IV}OL^2$(phen)] (**2**) ($10^{-4}$ M) in DMSO at different scan rates.

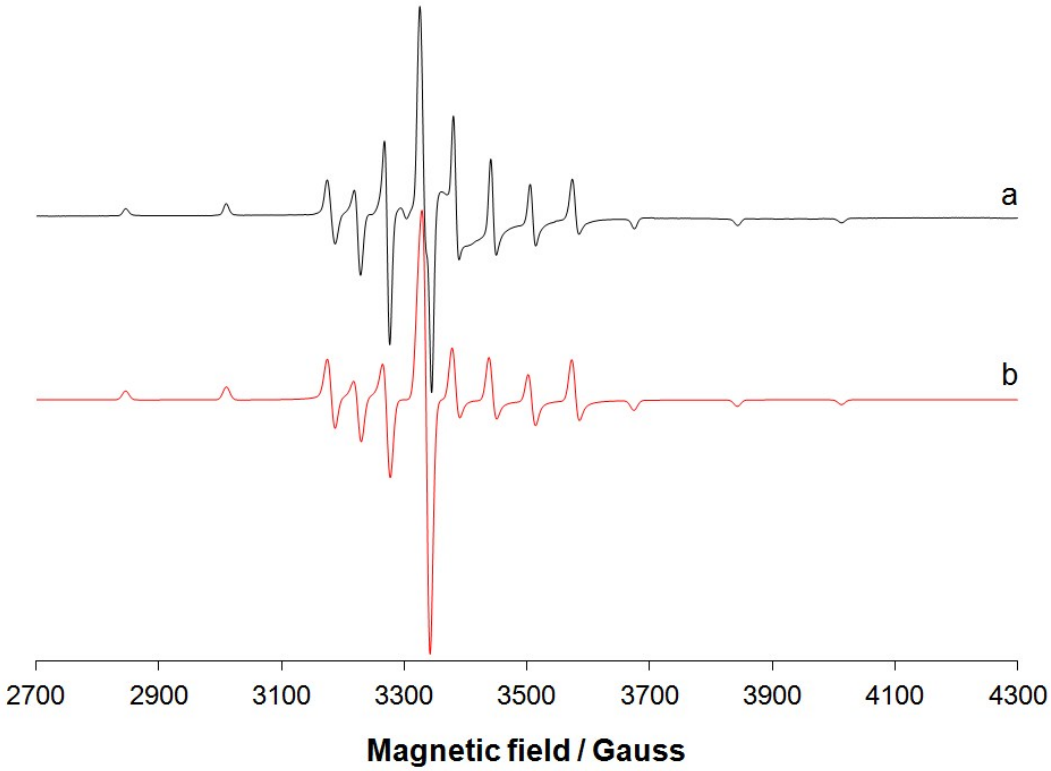


**Figure S10**. X-band anisotropic EPR spectra of the complex [$V^{IV}OL^2$(phen)] (**2**): (a) experimental spectrum in DCM and (b) generated spectrum with WinEPR software. The spectrum was generated with the spin Hamiltonian parameters reported in **Table 4** of the text.

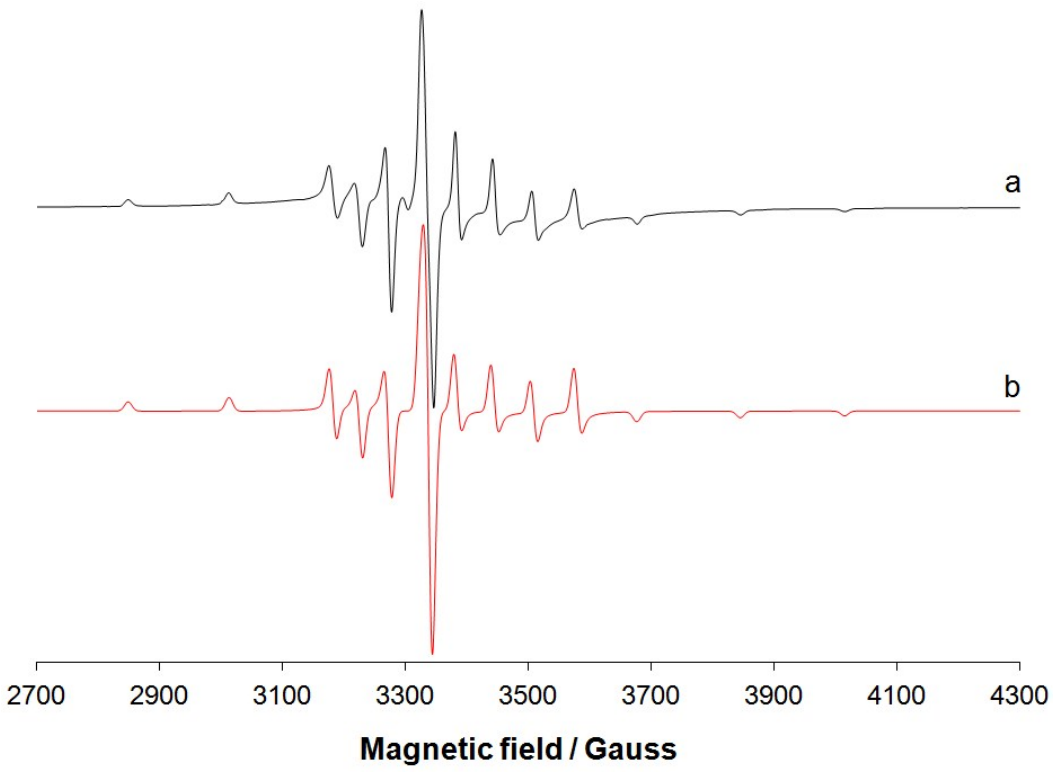


**Figure S11**. X-band anisotropic EPR spectra of the complex [$V^{IV}OL^{1}$(bipy)] (**3**): (a) experimental spectrum in DCM and (b) generated spectrum with WinEPR software. The spectrum was generated with the spin Hamiltonian parameters reported in **Table 4** of the text.

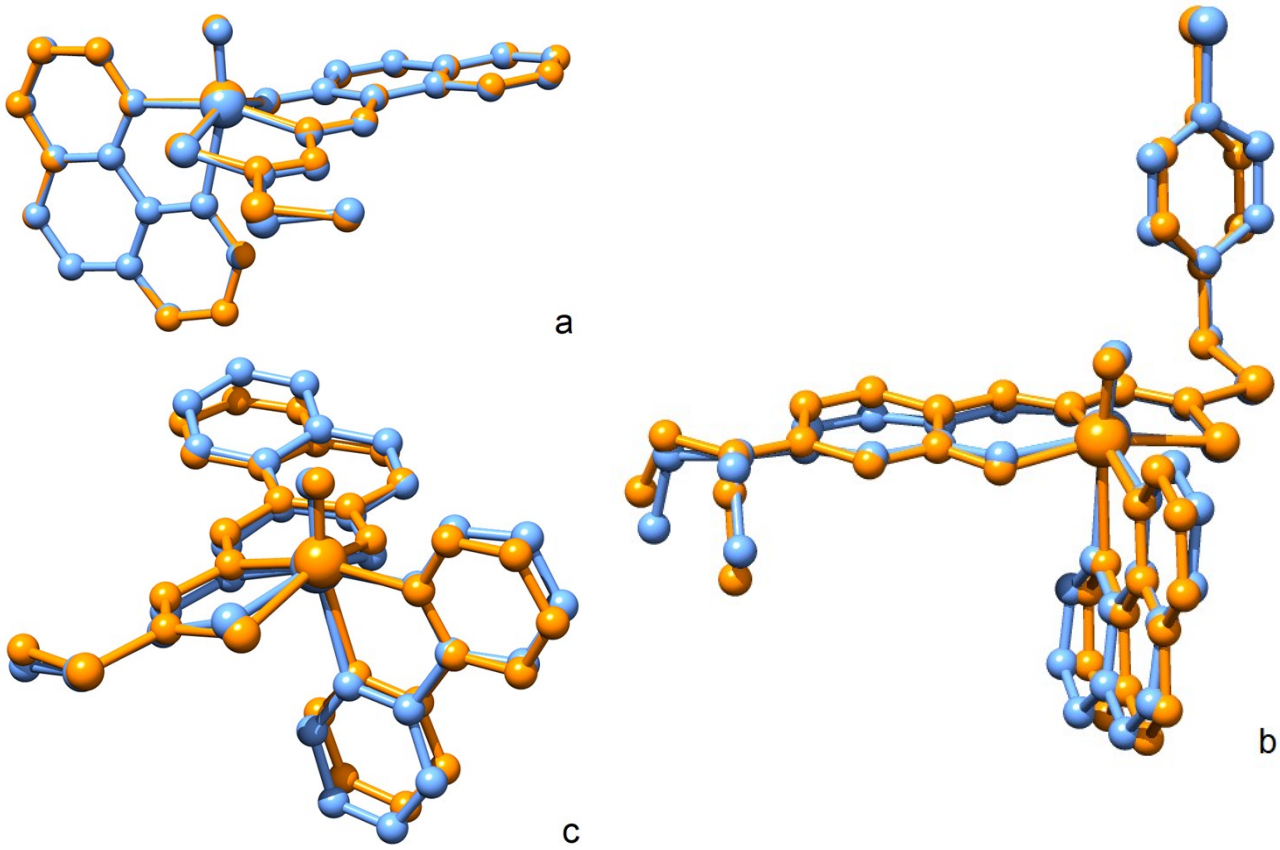


**Figure S12**. Superimposition of the X-ray (in blue) and DFT optimized (in orange) structures of the complexes: (a) [$V^{IV}OL^1$(phen)] (**1**); (b) [$V^{IV}OL^2$(phen)] (**2**) and (c) [$V^{IV}OL^1$(bipy)] (**3**).

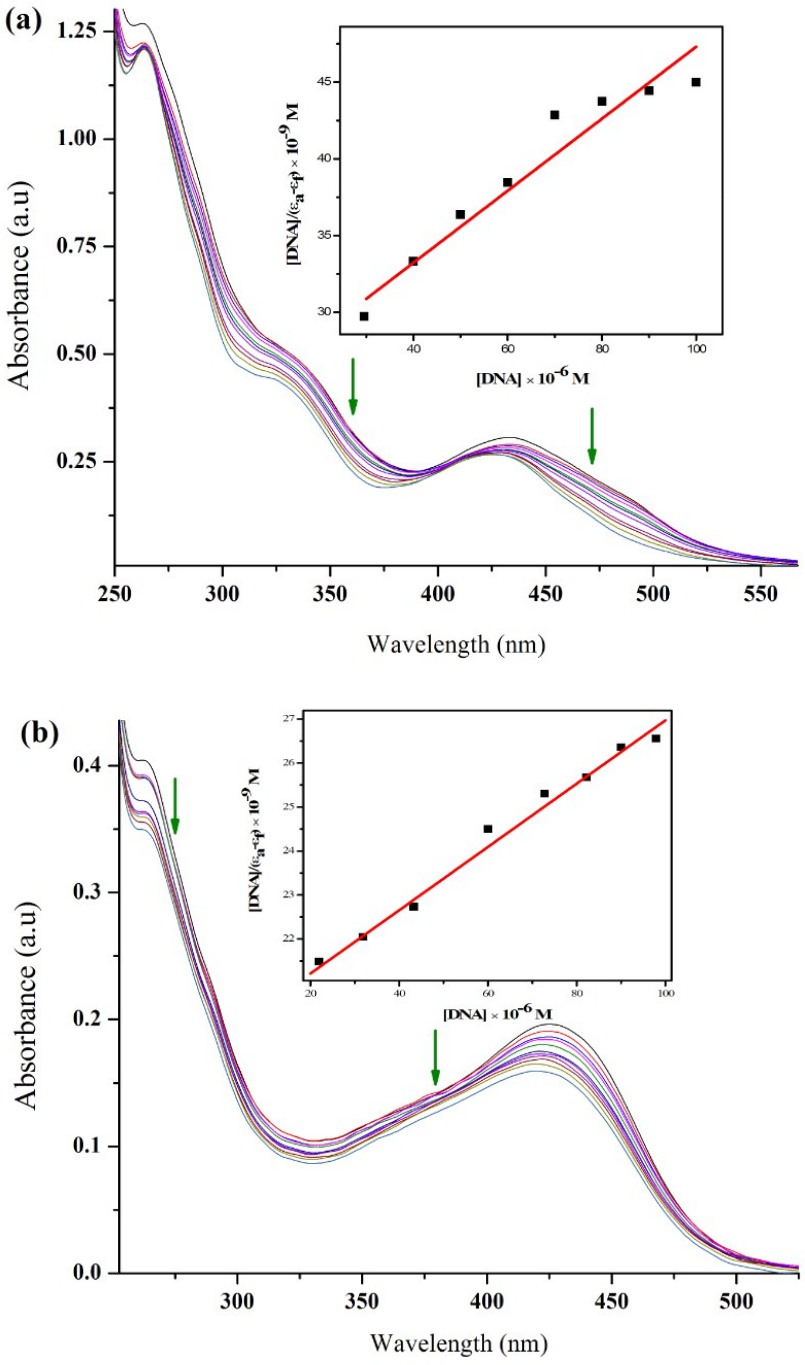


**Figure S13**. Absorption spectra of oxidovanadium(IV) complexes (25 µM each) in 50 mM Tris-HCl buffer at pH 8 upon the titration with CT-DNA (0–100 µM): (a) [$V^{IV}OL^1$(phen)] (**1**) and (b) [$V^{IV}OL^2$(phen)] (**2**). Arrows indicates the change in absorbance as function of the increase in the CT-DNA concentration. The inset shows the respective binding isotherm of complexes.

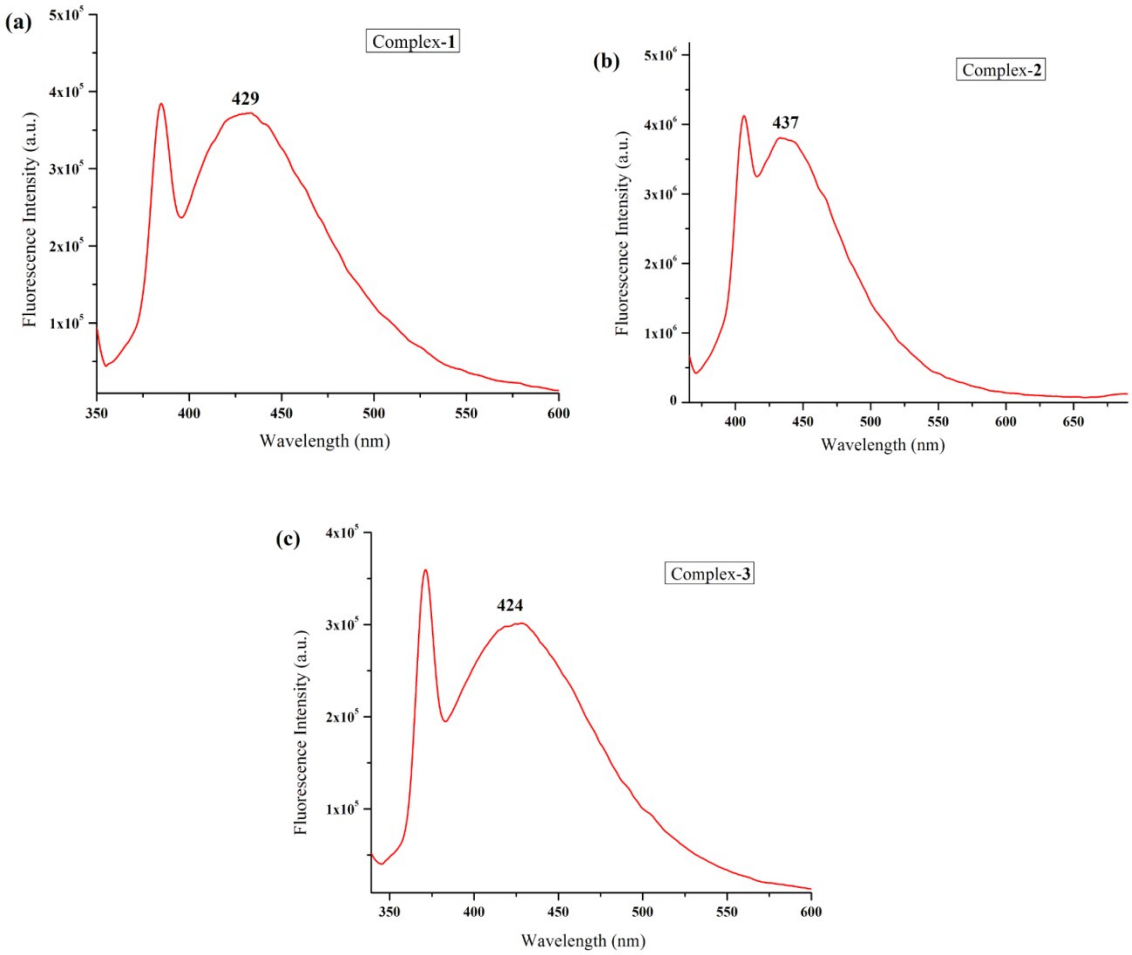


**Figure S14.** Fluorescence spectrum of [$V^{IV}OL^1$(phen)] (**1**) (a), [$V^{IV}OL^2$(phen)] (**2**) (b) and [$V^{IV}OL^1$(bipy)] (**3**) (c) in 50 mM Tris–HCl buffer.

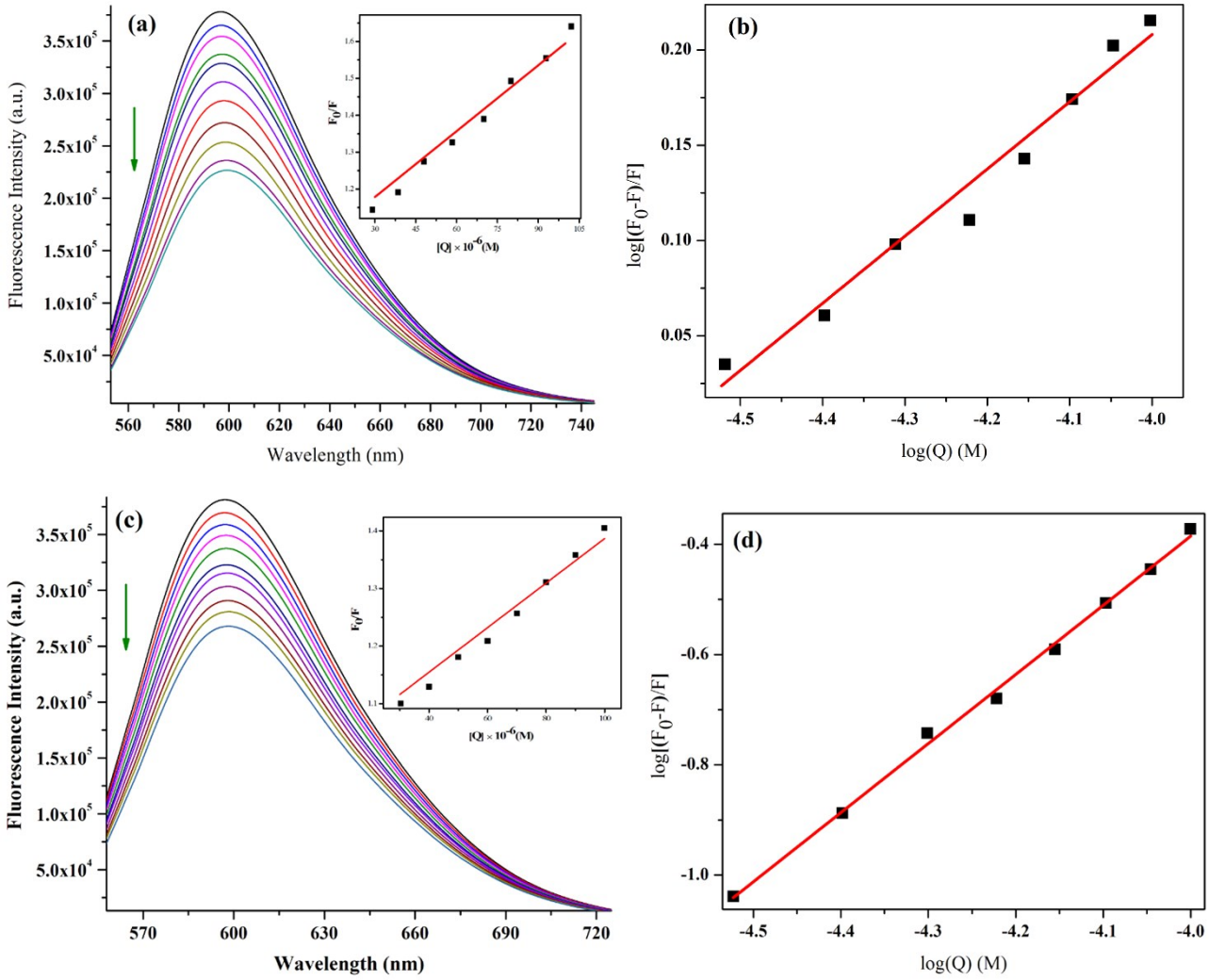


**Figure S15**. (a and c) EB (10 µM) displacement assay measuring the change in fluorescence intensity upon the titration of complex [$V^{IV}OL^1$(phen)] (**1**) and [$V^{IV}OL^2$(phen)] (**2**), respectively. Arrows indicates the change in fluorescence intensity as a function of the increase in the complex concentration (0–100 µM) and the insets represent the corresponding Stern-Volmer plot. (b and d) Scatchard plot of **1** and **2**, respectively.

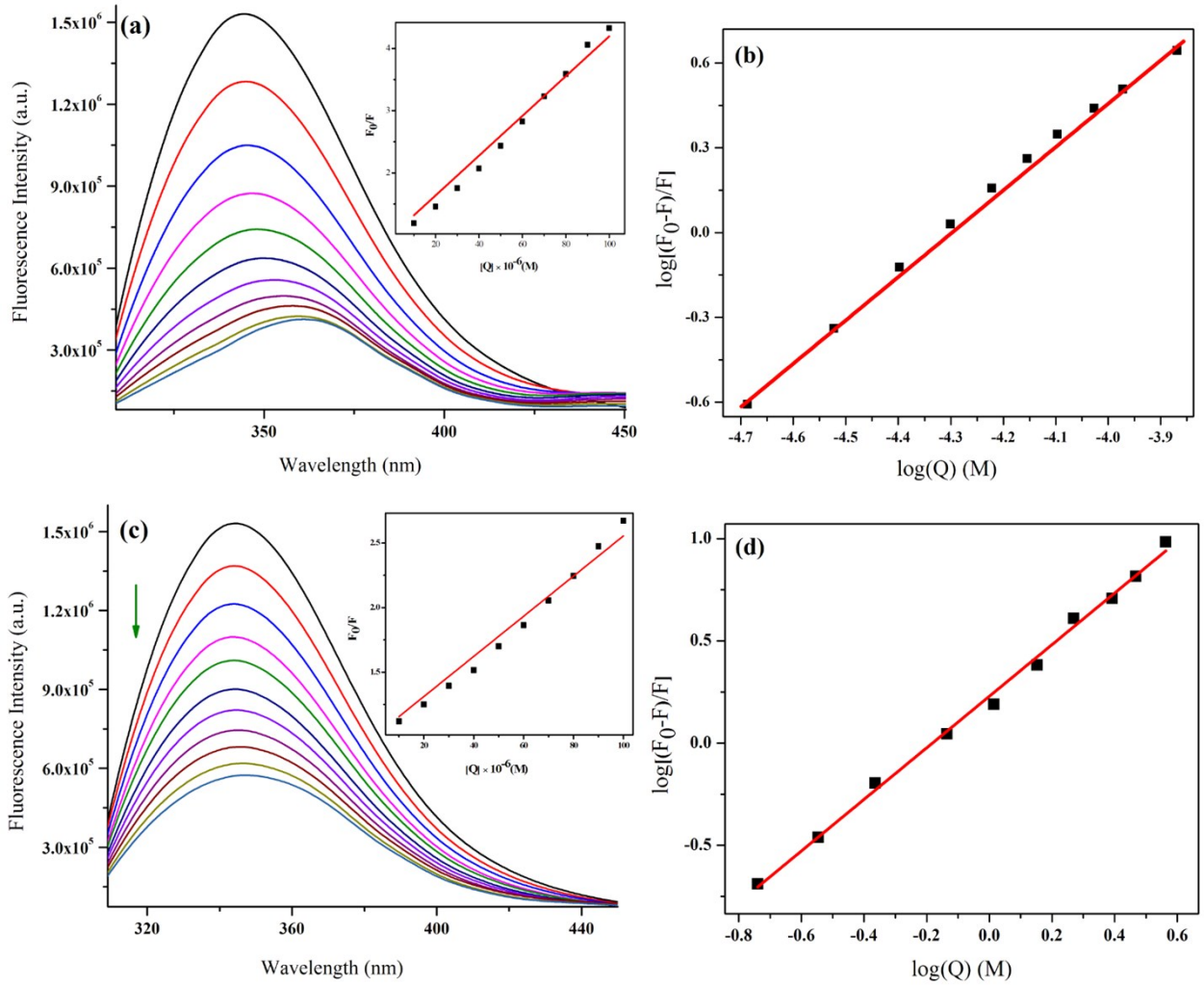


**Figure S16**. (a and c) Fluorescence quenching of HSA (10 µM) by complex [$V^{IV}OL^1$(phen)] (**1**) and [$V^{IV}OL^2$(phen)] (**2**), respectively. Arrows indicates the change in fluorescence intensity as a function of the increase in the complex concentration (0–100 µM) and the insets represent the corresponding Stern-Volmer plot. (b and d) represents the Scatchard plot of **1** and **2**, respectively.

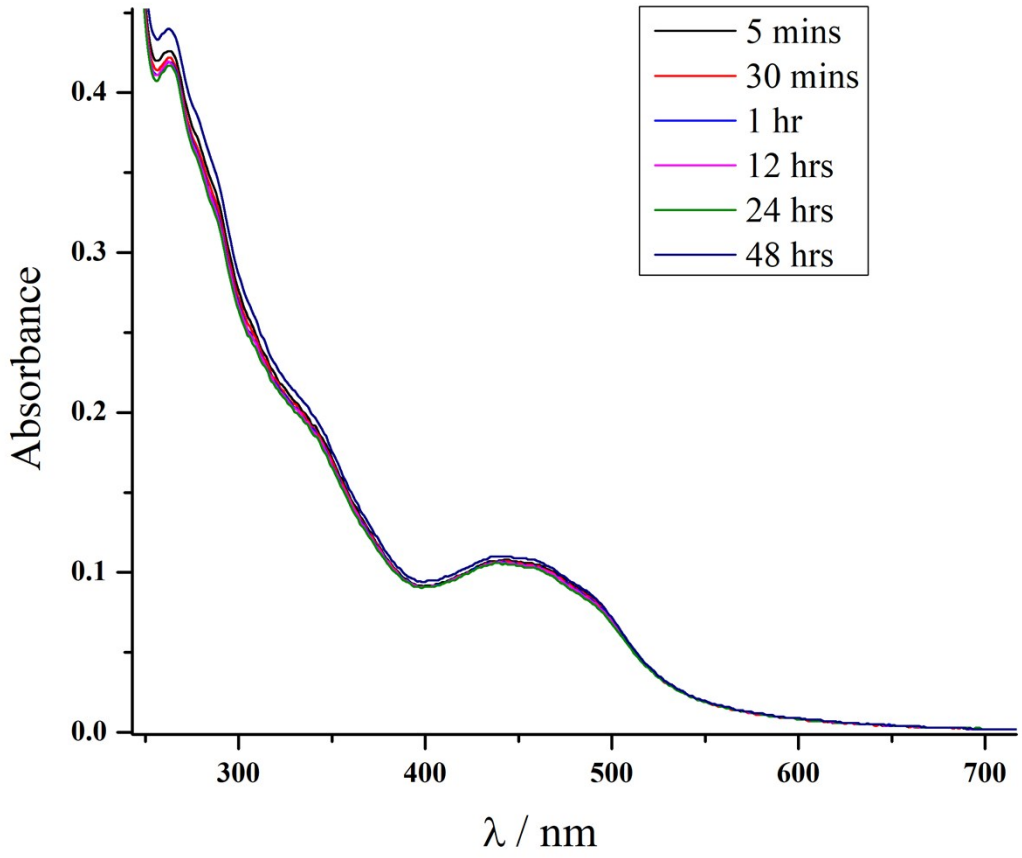


**Figure S17**. Time dependent UV/vis spectra of [$V^{IV}OL^{1}$(phen)] (**1**) in PBS buffer.